Earth and Planetary Science Letters 621 (2023) 118401

Contents lists available at ScienceDirect

Earth and Planetary Science Letters

journal homepage: www.elsevier.com/locate/epsl

The stability of cratons is controlled by lithospheric thickness, as evidenced by Rb-Sr overprint ages in granitoids

Eric D. Vandenburg [a,*], Oliver Nebel [a], Peter A. Cawood [a], R. Hugh Smithies [b], Fabio A. Capitanio [a], Laura A. Miller [a,c], Marc-Alban Millet [d], Emilie Bruand [e], Jean-François Moyen [f], Xueying Wang [a], Massimo Raveggi [a], Yona Jacobsen [a,g]

[a] School of Earth, Atmosphere and Environment, Monash University, Clayton, VIC 3800, Australia
[b] Department of Mines, Industry Regulation and Safety, Geological Survey of Western Australia, Perth, WA 6004, Australia
[c] Research School of Earth Sciences, Australian National University, Canberra, ACT 0200, Australia
[d] School of Earth and Environmental Sciences, Cardiff University, Cardiff, CF10 3AT, UK
[e] Geo-Ocean Department, Université Bretagne Occidentale, CNRS, Plouzané, 29280, France
[f] Université Jean-Monnet, Laboratoire Magmas et Volcans, UCA-CNRS-IRD, Aubière, France
[g] Faculty of Arts and Education, Deakin University, Burwood, Victoria 3125, Australia

ARTICLE INFO

Article history:
Received 15 July 2023
Received in revised form 30 August 2023
Accepted 11 September 2023
Available online xxxx
Editor: F. Moynier

Keywords:
in situ Rb-Sr
lithosphere-asthenosphere boundary
craton
crustal fluid flow
granitoid
far-field stress

ABSTRACT

The ancient cores of modern continents, cratons, are the oldest blocks of "stable" lithosphere on Earth. Their long-term survival relies on the resistance of their underlying thick, strong, and buoyant mantle keels to subsequent recycling. However, the effect of substantial geographical variations in keel thickness on the post-assembly behaviour and mass movement within these continental cores remains unknown. Here, we demonstrate that the spatial distribution of fluid-reset *in-situ* Rb-Sr ages for Paleo-Mesoarchean (3.6–2.8 billion years ago; Ga) granitoids of the Pilbara Craton, Australia shows remarkable correlation with independently-constrained lithospheric thickness models. Without craton-wide heating/magmatic events, these anomalously young Rb-Sr ages document episodes of fluid infiltration into granitoid complexes as a response to lithospheric reactivation by far-field stresses. This correlation implies that craton-wide fluid mobilization triggered by extra-cratonic Neoarchean to Mesoproterozoic (2.8–1.0 Ga) tectonic events is facilitated by variations in lithospheric strength and thickness. Compared to areas of older overprints, the two-thirds of the craton comprised of younger reset ages is underlain by comparatively thin lithosphere with higher susceptibility to reactivation-assisted fluid flow. We propose that even the strongest, most pristine cratons are less stable and impermeable than previously thought, as demonstrated by the role of granitoid complexes and cratons as selective lithospheric "sponges" in response to minor tectonic forces. Therefore, variations in lithospheric thickness, likely attained before cratonization, exert a crucial control on billions of years of fluid movement, elemental redistribution and mineralization within ancient continental nuclei.

1. Introduction

At least three-quarters of the present-day volume of continental crust is inferred to have been produced in the Archean Eon (4.00–2.50 Ga) (Dhuime et al., 2012). However, outside of the scarce remnants restricted to cratons, the oldest stable blocks of Earth's lithosphere, most of this crust no longer exists in its original form. The survivability of these cratons following their stabilization and amalgamation (a process commonly referred to as "cratonization") requires the resistance of the cratonic subcontinental lithospheric mantle (SCLM) to subsequent reworking and modification events. Previous studies have highlighted the importance of its chemical buoyancy imparted by higher degrees of melt extraction in a hotter Archean mantle (e.g., Herzberg and Rudnick, 2012; Jordan, 1988), its higher viscosity compared to Phanerozoic lithosphere (e.g., Capitanio et al., 2020; Lenardic and Moresi, 1999; Sleep, 2003) and its higher integrated yield strength (e.g., Cooper et al., 2006) as intrinsic factors that contribute to the long-term stability of Archean lithosphere. However, this may not be suf-

* Corresponding author.
E-mail address: eric.vandenburg@monash.edu (E.D. Vandenburg).

https://doi.org/10.1016/j.epsl.2023.118401

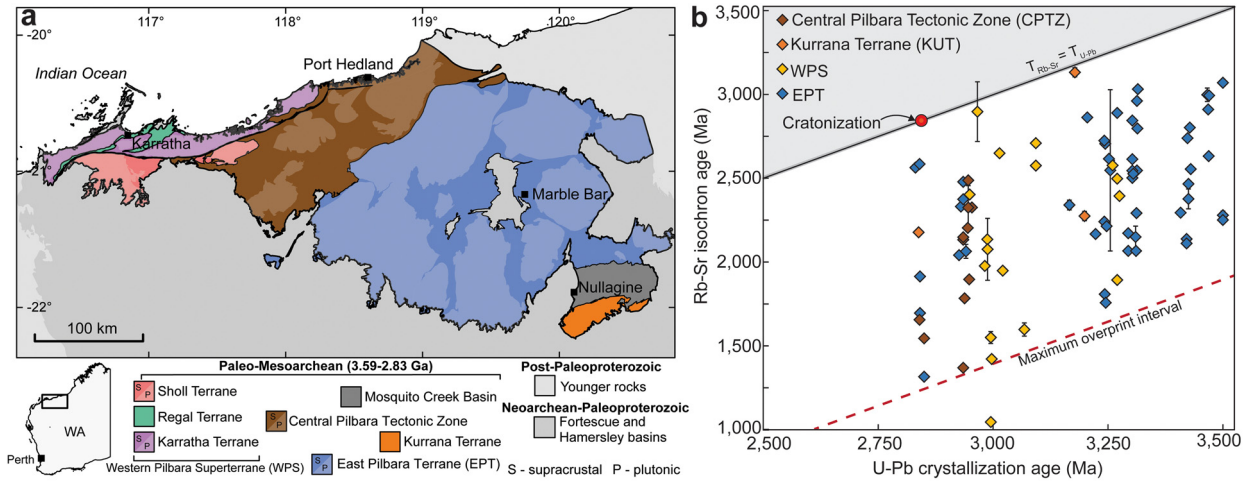

Fig. 1. Geological map of the Pilbara Craton and comparative U-Pb and Rb-Sr ages of Pilbara Craton granitoids. **a**, Simplified geological map of the Pilbara Craton, illustrating the lithotectonic subdivisions of the craton. Lighter-shaded regions in the craton represent granitoid complexes and plutons. Map adapted from (Martin et al., 2015). **b**, Plot of in-situ Rb-Sr ages in biotite and feldspar versus their corresponding compiled U-Pb magmatic crystallization age in zircon for Pilbara granitoids analyzed in this study. Only two samples have Rb–Sr ages within 2σ uncertainty of zircon U–Pb ages (solid black line). Fences denote 2σ uncertainty on Rb-Sr ages. The shaded area in grey denotes the "zone of implausibility," i.e., Rb-Sr ages that are implausibly older than U-Pb crystallization ages. The dashed line corresponds to the interval of maximum overprint, i.e., ΔMyr = 1500 Myr. Abbreviations: CPTZ – Central Pilbara Tectonic Zone, EPT – East Pilbara Terrane, KUT – Kurrana Terrane, MCB – Mosquito Creek Basin, WPS – Western Pilbara Superterrane.

ficient to explain craton longevity, as evidence of reworking and recycling is widespread (e.g., Lee et al., 2011; Bedle et al., 2021), showing that protection from subduction, rifting and mantle plume events is also essential in cratonic preservation, as these are associated with significant metasomatism and destruction of cratonic lithosphere (e.g., Liu et al., 2019). Cratonic lithosphere is broadly agreed to be produced by relatively shallow melting of the mantle, with subsequent thickening via compression and accretion during amalgamation (e.g., Capitanio et al., 2020; Pearson et al., 2021). However, significant debate remains regarding the regimes conducive to cratonic lithosphere formation (Cawood et al., 2022); this nearly includes the entire tectonomagmatic spectrum, ranging from short-lived rifting associated dehydration stiffening and lithospheric stacking in non-plate tectonic environments (Capitanio et al., 2020; Vandenburg et al., 2023), to oceanic subduction accompanied by arc-continent collision (Perchuk et al., 2020), and upwellings (Lee et al., 2011). Thus, the conditions favourable for forming cratonic lithosphere in the Archean may be non-unique, only sharing a common result: buoyant, rigid lithosphere with greater strength than its Phanerozoic counterparts.

The spatio-temporal distribution of tectonothermal events within the crust is demonstrably related to lithospheric strength (e.g., Poudjom Djomani et al., 1999). In the context of cratons, post-stabilization tectonothermal events are generally the result of far-field tectonic stresses from bounding orogens (Flowers et al., 2008), which will be focused into weaker and marginal areas, where strain will be localized (Braun and Shaw, 2001; Raimondo et al., 2014). Because thickness exerts a significant control on the strength of the continental lithosphere (e.g., Bedle et al., 2021; Steinberger and Becker, 2018; Tesauro et al., 2012), the susceptibility of each portion of a craton to subsequent tectonothermal overprint is likely a function of the underlying depth to the lithosphere-asthenosphere boundary (LAB).

Despite previously falling out of favour (Liebmann et al., 2022), the geochronological application of the Rb-Sr isotopic decay system has undergone a renaissance in recent years due to the analytical elimination of isobaric interferences on the radiogenic daughter isotope (^{87}Sr) and the respective parent isotope (^{87}Rb) (Hogmalm et al., 2017; Zack and Hogmalm, 2016), enabling the precise *in-situ* dating of biotite and plagioclase pairs. Due to their low reset temperatures compared to zircon chronometers and their susceptibility to fluid-borne alteration, mica-controlled Rb-Sr isochron ages may have the sensitivity to track subtle variations in crustal temperatures, metamorphism, and metasomatic alteration. Because of the relatively low closure temperatures of plagioclase and biotite ($T_C \approx 300–500\,°C$) (Dodson, 1973; Willigers et al., 2004) even compared to the whole-rock Rb-Sr system ($T_C \approx 700\,°C$ in felsic systems; e.g., Harrison et al., 1979), the mineral isochron method is quite sensitive to thermal overprints. Furthermore, Rb and Sr are both readily mobilized by fluids (e.g., Attendorn and Bowen, 1997), making the system susceptible to metasomatic overprint. While these features can pose issues when attempting to date magmatic events with this method, it makes for an effective tool for precisely dating low-level thermal and metasomatic events that are not detectable by other geochronological methods (e.g., Bhaskar Rao et al., 1992; Tillberg et al., 2021; Wang et al., 2022).

Here, we present new in-situ Rb-Sr geochronology data from biotite and feldspar in 81 granitoids from the Pilbara Craton of Western Australia with well-defined emplacement ages ranging from 3.50–2.83 Ga. With this, we test the role of cratonic lithospheric thickness in controlling the spatio-temporal distribution of tectonothermal overprints. The Pilbara is one of the oldest, least deformed and most pristine cratons on Earth, providing a relatively complete record of crustal evolution from the early Paleoarchean to the late Mesoarchean (Hickman, 2023) (Fig. 1a). The craton comprises six main lithotectonic blocks: the East Pilbara Terrane (EPT), the Karratha, Regal, and Sholl terranes, collectively referred to as the West Pilbara Superterrane (WPS), the Central Pilbara Tectonic Zone (CPTZ), and the Kurrana Terrane. The cratonization of the Pilbara at ca. 2.85 Ga (Hickman, 2023), combined with the lack of subsequent reworking and large-scale deformation events, makes this craton a prime candidate to study the pre- and post-cratonization tectonic history of Archean cratons and the influence of amalgamation mechanisms on lithospheric thickness. Our samples range in composition from sanukitoid (high-Mg diorite) to tonalite-trondhjemite-granodiorite (TTG) series and potassic granite lithologies with magmatic crystallization ages spanning 3.50–2.83 Ga. The majority of samples are undeformed with equigranular textures. However, the fabrics in deformed samples correlate to pre-cratonization deformation events (Hickman, 2023) (Fig. 2a); thus, any post-2.85 Ga isochron ages derived from Rb-Sr

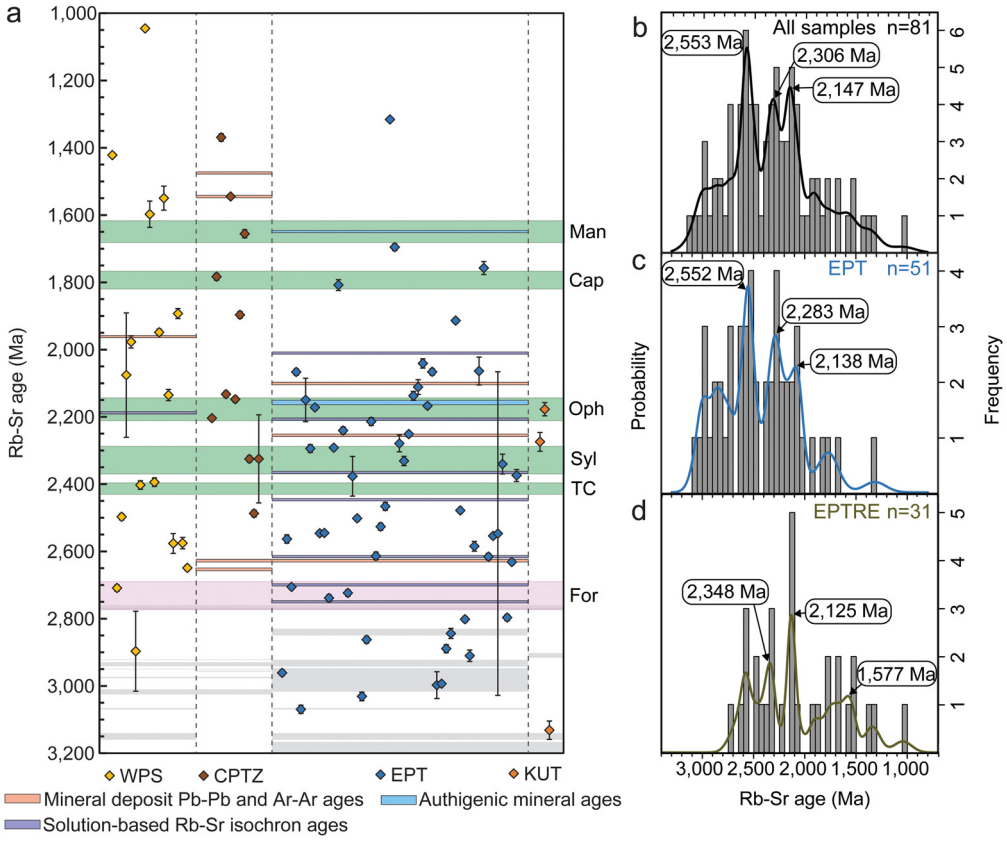

Fig. 2. Temporal distributions of in-situ plagioclase and biotite Rb-Sr ages. **a**, Rb-Sr ages from this study divided by lithotectonic block. Grey-shaded areas correspond to fabric-forming deformation events in Pilbara granitoids (Hickman, 2023). The pink shaded area corresponds to the duration of the Fortescue Large Igneous Province (For) (Mole et al., 2018), whereas the green shaded areas correspond to the durations of the Turee Creek (TC) (Bekker et al., 2020), Sylvania (Syl) (Rasmussen et al., 2022), Ophthalmia (Oph) (Rasmussen et al., 2023), Capricorn (Cap) (Thorne and Trendall, 2001), and Mangaroon (Man) (Sheppard et al., 2005) orogenies. The orange, purple and blue shaded areas correspond to previously constrained post-Mesoarchean Ar-Ar and Pb-Pb ages of Archean mineral deposits (Huston et al., 2002), solution-based Rb-Sr isochron ages (Rasmussen et al., 2005, 2022; Oversby, 1976), and authigenic mineral metamorphic U-Pb ages (Rasmussen et al., 2005, 2007) from the exposed portions of the Pilbara Craton, respectively. Fences denote 2σ uncertainty on ages. **b**, Kernel density and histogram plot of all Rb-Sr ages from this study, highlighting the age peaks within the dataset. **c**, Kernel density and histogram plot of Rb-Sr ages from the EPT, illustrating the relative similarity of this subset to the whole dataset. **d**, Kernel density and histogram plot of Rb-Sr ages from areas affected by the East Pilbara Terrane Rifting Event (EPTRE), illustrating the younger distribution of ages relative to the entire dataset and the EPT subset. Bin and kernel widths are 50 Myr. Abbreviations: CPTZ – Central Pilbara Tectonic Zone, EPT – East Pilbara Terrane, KUT – Kurrana Terrane, WPS – Western Pilbara Superterrane.

isotope analysis reflect or are at least affected by the reactivation but not the formation, of these fabrics.

2. Methods

2.1. In-situ Rb-Sr geochronology

Over six analytical sessions, the Rb-Sr ages of plagioclase, alkali feldspar and biotite were collected on mineral separate pucks at the Isotopia Laboratory, Monash University, Australia. Data for all analyses was acquired using an ASI-RESOlution ArF 193 nm excimer laser equipped with a dual volume Laurin Technic S155 ablation cell coupled to a ThermoFisher iCAP-TQ quadrupole ICP-MS. Analyses of unknowns were corrected for fractionation of Rb–Sr using repeat analysis of standard reference materials (NIST-610, Mica-Mg pressed powder pellets and in-house natural mica) that together yield a ±2.5% reproducibility of the Rb/Sr ratio; Therefore, uncertainties on individual measurements of $^{87}Rb/^{86}Sr$ and $^{87}Sr/^{86}Sr$ are 2.5% at the 95% confidence level (2SE). The weighted mean Rb-Sr ages used in this study have 95% confidence limits. The complete analytical procedures are detailed in the Supplementary Information, whereas analyses of primary standards, secondary reference materials, and complete datasets are provided in Tables S1-S3.

2.2. Compiled U-Pb geochronology, ΔMyr calculation, and trace element data

Data for the U-Pb in zircon-derived magmatic crystallization age map was taken from the literature (Table S4). For each sample, ΔMyr equals the Rb–Sr age subtracted from the appropriate magmatic unit's established U–Pb zircon age. The whole-rock geochemical data of the Pilbara granitoids was taken from the literature (Table S5). Refer to the Supplementary Information for further details.

2.3. Interpolation methods and classification schemes

Isotopic age contour maps were constructed in ArcGIS Pro using the inverse distance-weighted interpolation function of the Spatial Analyst toolbox, with class intervals constructed using the geographic interval classification scheme. Input parameters included a power of 2, a variable search radius, and 15 maximum points. We refer the reader to the Supplementary Information for a detailed description of the methodology.

3. Results

The age populations of our analyzed samples are complex (Figs. 1b, 2; Figs. S1-S7; Table S6). Out of 81 ages, only one of

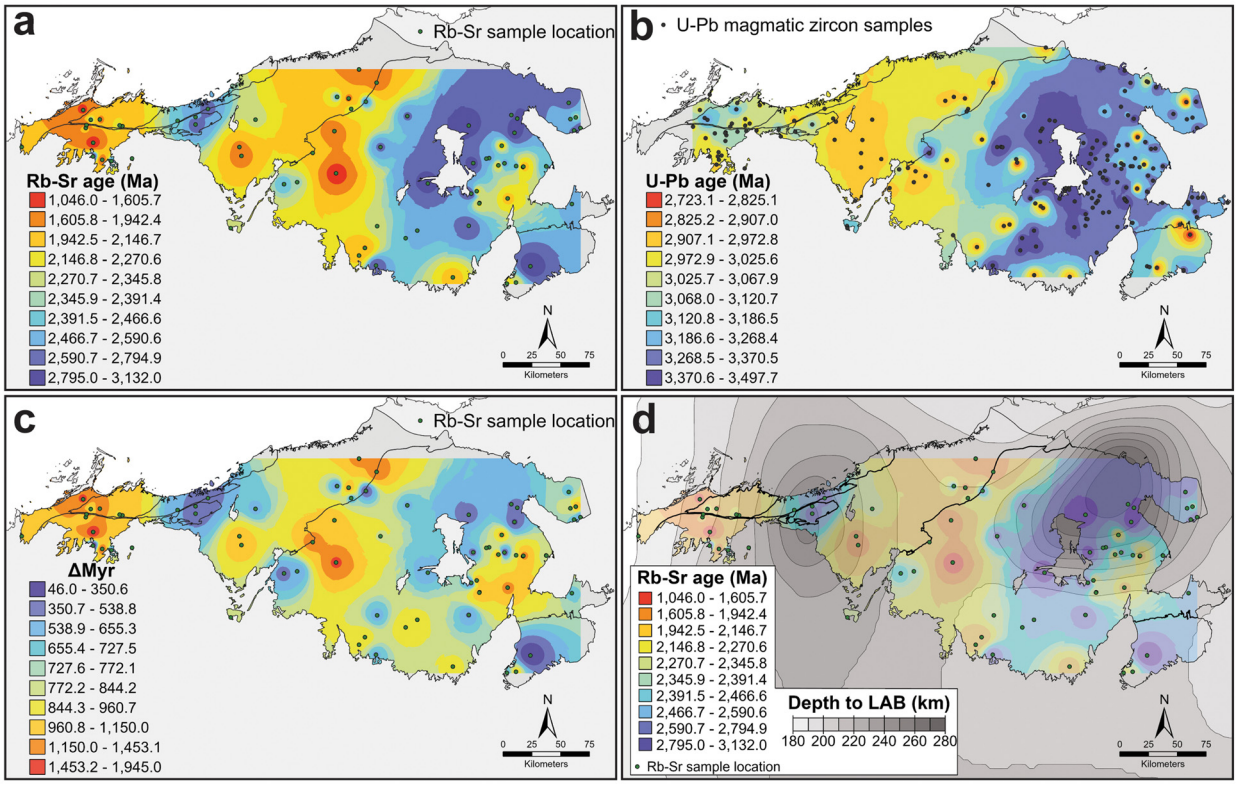

Fig. 3. Isotopic age contour and lithospheric thickness maps of the Pilbara Craton. **a**, Contour map of in-situ plagioclase and biotite Rb-Sr ages from this study. Relatively old Rb-Sr ages (blue) comprise the eastern portion of the EPT and the central portion of the WPS, whereas the western margin of the EPT and the CPTZ are characterized by younger ages (orange-red hues). **b**, Contour map of compiled magmatic U-Pb zircon crystallization ages. The granitic domes of the EPT and the WPS contain the oldest ages (blue hues); the ages within the EPT progressively young towards the western margin of the block. The youngest ages (orange-red hues) are located within a large portion of the CPTZ and as minor blips on the margins of the EPT and Kurrana Terrane. Sample ages can be found in Table S4. **c**, Contour map of ΔMyr, the difference between the magmatic U-Pb age of a sample and its Rb-Sr metamorphic overprint age (in millions of years). Colours indicate the duration of the time interval between crystallization and the last recorded reset (blue = short, red = long). The patterns are essentially the same as in b, except for small high zones concentrated along the margins of the EPT due to these samples' older age (>3.25 Ga). **d**, Contour map of Rb-Sr ages overlain onto the CRWF14 Australian continent lithosphere-asthenosphere boundary (LAB) depth model of Czarnota et al. (2014), derived from FR12 seismic tomography (Fishwick and Rawlinson, 2012). Zones of older Rb-Sr reset ages broadly correspond to areas of thicker lithosphere (darkest grey hues), whereas zones of younger Rb-Sr reset ages correspond to areas of thinner lithosphere (lightest grey hues). Note that the lithospheric thickness is still within reason for that of a craton. Solid lines within contour maps demarcate the boundaries of each lithotectonic block.

the samples records primary magmatic Rb-Sr crystallization ages, albeit with an offset of 46 million years (Myr) to a younger age, most likely due to cooling (Fig. 1b). The other samples record much younger ages that can only be interpreted as reset ages ranging from 3.13 to 1.05 Ga (Figs. 1b, 2; see Tables S1-S3 for materials for isochron construction). Only four samples yield Rb-Sr ages that predate cratonization at 2.86 Ga; Most samples experienced an overprint at some point after this, forming broad age populations with peaks at 2.56 Ga, 2.31 Ga, and 2.15 Ga (Fig. 2b).

In areas subjected to greenschist facies metamorphism, it is common for plutonic rocks to have younger Rb-Sr biotite ages than their igneous U-Pb zircon ages due to the difference in closure temperature between the two systems (~450 °C) (Carlson, 2011). What is surprising for the Pilbara dataset, however, are the time differences of up to 1.95 Gyr between crystallization and the final reset, well after the last regional metamorphic event that affected the exposed portion of the craton. In addition to their lack of macroscopic veins, the samples have whole-rock alteration index values consistent with those of least altered intermediate-acidic igneous rocks on a global scale, thereby ruling out a high-temperature metasomatic/hydrothermal origin to the reset ages (Fig. S8).

The regional differences in Rb-Sr age distributions observed on kernel density plots suggest a geographic control on the ages of overprints. For example, while the age distribution of the subset from the East Pilbara Terrane (EPT) is similar to those of the entire dataset (Fig. 2b, c), areas affected by the 3.22–3.18 Ga East Pilbara Terrane Rifting Event (e.g., Vandenburg et al., 2023) (EPTRE; easternmost EPT, the CPTZ and the Sholl Terrane; Fig. 2d), have a distribution towards younger ages, with a plurality of samples affected by the Ophthalmia Orogeny, albeit with a slightly younger peak (2.13 Ga).

Investigation of all reset ages in a spatial context reveals a pattern broadly resembling some of the prominent geologic features recorded by the Pilbara Craton. Rb-Sr age contour maps show significant crustal block-parallel spatial variations in reset ages, also visible in the U-Pb zircon age contour map (Fig. 3a, b). The CPTZ, most of the WPS, and the western EPT have reset ages predominantly younger than 2.3 Ga. In contrast, the northeastern EPT and the easternmost Sholl Terrane overwhelmingly have reset ages greater than 2.5 Ga. These spatial variations are also reflected in the contour map displaying the difference between magmatic crystallization and metamorphic overprint ages (expressed as ΔMyr) (Fig. 3c); areas with older reset ages have shorter time intervals between crystallization and the last recorded overprint, compared to areas of younger reset ages. Notably, neither the relative proximity of samples to major faults nor the orientation of the faults themselves appears to exert a control on the reset ages, as evidenced by the distance of samples from damage zones and the scatter on plots of reset age versus the azimuth of the closest fault to a sample, respectively (Fig. S9). Thus, large-scale structural factors must not exert a first-order control on the geographic distribution of the overprint ages observed in our samples.

Despite the lack of macroscopic evidence for deformation and alteration in samples, examination of thin sections reveals ample microscopic evidence for alteration and brittle deformation (Fig. S10). In altered samples, the assemblage is consistent with semi-pervasive to pervasive propylitic alteration; this predominantly consists of sericite and epidote after plagioclase, which partially or fully replaces crystal rims and cores, and chlorite after biotite, with partial to complete replacement of crystals. The lack of recrystallization in biotite suggests that resetting the Rb-Sr system is related to diffusion. Deformation structures unrelated to macroscopic fabrics appear characteristic of a brittle regime (e.g., Groshong, 1990). These include <200 μm-wide en-echelon veinlets and twin-parallel fractures in plagioclase, <100 μm-wide transgranular fractures in quartz, microcline, and plagioclase, and <1.5 mm-wide fracture zones comprised of alteration minerals and recrystallized albite. Many of these features form a sparse interconnected network; extensive sericitization along fracture planes in plagioclase suggests that this network facilitated fluid flow (e.g., Fitz Gerald and Stünitz, 1993).

4. Discussion

Although we can exclude a high-temperature origin of the overprint ages, this does not rule out overprint by relatively low-temperature (but >250 °C) fluids, likely ingressed into the crust due to structural reactivation associated with far-field orogenic events. Notably, there is no evidence for craton-wide (*sensu-lato*) heating events and associated magmatic activity after the cessation of the Fortescue LIP at 2.69 Ga; thus, these overprint ages necessitate derivation from low-temperature fluid-rock interactions associated with crustal fluid flow events triggered by extra-cratonic far-field stresses. During orogenic events, compressive tectonics can drive fluids from the deformation front into the adjacent crust down pressure gradients, akin to a "squeegee" (e.g., Cox, 2005; Oliver, 1992), further enhanced by lateral variations in thermal gradients (Lyubetskaya and Ague, 2009). This notion is not far-fetched; the Rb-Sr ages of veins in the Fennoscandian Shield from localities hundreds of kilometres apart correlate with fluid flow and fracture reactivation events initiated by far-field orogens (Tillberg et al., 2021). Furthermore, in the (unexposed) central and southern portions of the Pilbara Craton, multiple syn-orogenic fluid flow events affected the overlying Fortescue and Hamersley basins during the Proterozoic (e.g., Fielding et al., 2017; Rasmussen et al., 2005, 2022, 2023; Brown et al., 2004; White et al., 2014). The fluids mobilized during these events were relatively neutral and saline, achieved a maximum temperature of 375 °C in the overlying basins and travelled along bedding-parallel fractures, basinal faults, and lava flowtops (Rasmussen et al., 2023; Brown et al., 2004; White et al., 2014). These events are associated with propylitic alteration (calcite, chlorite, sericite, ± quartz) and are responsible for the overprint of authigenic monazite and xenotime during the Turee Creek, Sylvania, Ophthalmia and Mangaroon orogenies (e.g., Fielding et al., 2017; Rasmussen et al., 2005, 2022, 2023). The kernel density diagrams of our results further support overprint by far-field stress-triggered craton-wide crustal fluid flow events, coinciding the 2.37–2.29 Ga Sylvania and 2.20–2.15 Ga Ophthalmia orogenies (Fielding et al., 2017; Rasmussen et al., 2005, 2022, 2023) but also with a previously undescribed event at 2.56 Ga (Fig. 2a).

In order to travel into the exposed portion of the craton, these fluids would have to flow through the deeper Archean faults and structural corridors concealed beneath the basins, thereby imparting the fluid temperatures required to overprint the Rb-Sr system despite being further from the deformation front. Because the propylitic alteration assemblages associated with the ingress of >250 °C fluids (Rasmussen et al., 2023) would be somewhat identical to regional greenschist facies metamorphism (Pirajno, 2009), it is not readily identified in hand sample, nor is it likely to be detected using the alteration box plot method (Fig. S8). As demonstrated in Figure S10, fractures and veins associated with post-Fortescue deformation in Pilbara granitoids are only identified in thin sections (e.g., Wiemer et al., 2016). Nevertheless, as illustrated in Fig. 2a, multiple lines of evidence indicate that the fluids did travel this far. First, dissolution-based Rb-Sr analysis of plagioclase and biotite from EPT granitoids by Oversby (Oversby, 1976) yielded ages between 2.75 and 2.01 Ga, indicating post-crystallization disturbance. Second, several vein-hosted mineral deposits in the exposed Archean portions of the craton yield Pb-Pb model and K-Ar ages between 2.63 and 1.48 Ga (Huston et al., 2002). Third, Rasmussen et al. (2007) identified 2.16 and 1.65 Ga growth events in metamorphic monazite from Soanesville Group shales in the EPT, associated with minor chlorite infill along bedding planes. Similar events were also identified in the northeast portion of the craton (Sheppard et al., 2017).

The patterns within the Rb-Sr contour maps show a strong correlation with the CRWF14 Australian continent LAB model of Czarnota et al. (2014), derived from FR12 regional isotropic V_S seismic tomography of Fishwick and Rawlinson (2012) (Fig. 3d). Other Australian LAB models (e.g., mantle xenolith and xenocryst thermobarometer-calibrated models of Hoggard et al., 2020) lack the resolution to elucidate lithospheric thickness beneath the Pilbara Craton (the lack of xenoliths/xenocrysts from the Pilbara in the calibration method likely leads to incorrect LAB contour values in this region). Therefore, we consider the CRWF14 model to be the most accurate representation of the actual depth of the LAB for the Pilbara Craton. Although this model has limited resolution, it agrees with the results of the Rb-Sr contour mapping, demonstrating that the distribution of areas with older overprints correlates with thicker lithosphere, which is ultimately influenced by diverse tectonomagmatic settings. Extra-cratonic stresses will be focused into areas of thinner, weaker lithosphere, which are less resistant to structural reactivation-triggered crustal fluid flow events (Poudjom Djomani et al., 1999; Flowers et al., 2008; Braun and Shaw, 2001; Raimondo et al., 2014; Tesauro et al., 2012; Cox, 2005) (Fig. 4). Thus, Rb-Sr overprinting continues in these weaker areas until other lithotectonic blocks encircle the craton via accretion/docking, sufficiently separating the craton from convergent plate margins to act as a buffer from far-field stresses (Bedle et al., 2021; Tillberg et al., 2021). Our study is the first instance of a demonstrable correlation between Rb-Sr ages and lithospheric thickness; this suggests that Rb-Sr isotope mapping is a potential method of independently verifying LAB models derived from geophysical methods.

Areas with older Rb-Sr overprint ages (>2.5 Ga) substantially correspond to blocks of thick, rigid lithosphere that had been constructed prior to the EPTRE, in addition to younger lithosphere produced by localized zones of high degree mantle melting (i.e., the ca. 2.95 Ga komatiitic basalts of the Bookingarra Group in the far-east Sholl Terrane) (e.g., Vandenburg et al., 2023; Smithies et al., 2004). In contrast, regions with younger Rb-Sr overprint ages (<2.3 Ga) largely correspond to lithosphere underlying blocks of thin, juvenile crust created during or after the EPTRE (as well as thinned lithosphere). Therefore, the relatively thin, juvenile lithosphere areas are more susceptible to post-cratonization metamorphic overprint from outboard tectonic events than zones of thicker lithosphere, even though both have been subject to some degree of post-emplacement overprints.

In the upper crystalline crust, the bulk permeability that facilitates crustal fluid-flow events requires structural reactivation (Siler and Kennedy, 2016; Townend and Zoback, 2000). Therefore, areas that accommodate far-field tectonic stresses (i.e., thinner, weaker lithosphere) will experience these fluid overprint events, whereas

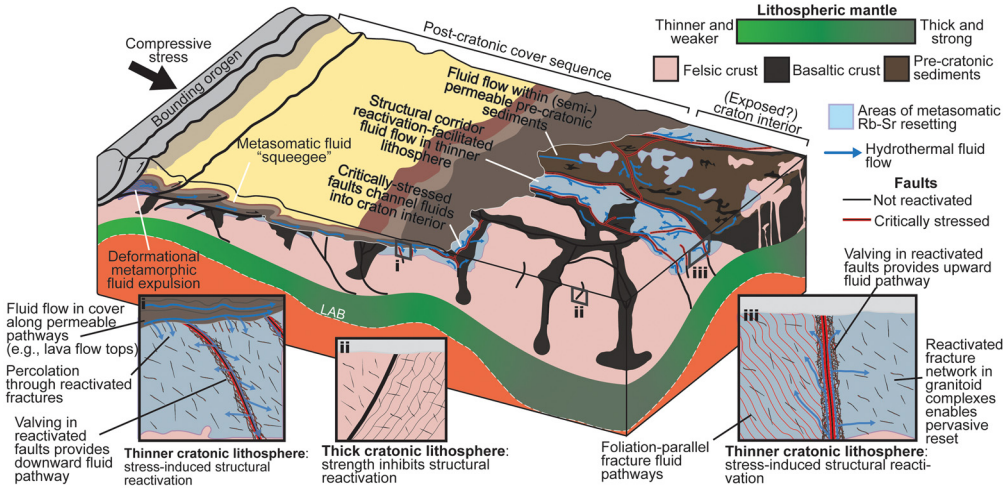

Fig. 4. Cratonic lithosphere thickness controls the age of metasomatic overprints. Schematic diagram illustrating the controls that lithospheric thickness and strength exert on the distribution of Rb-Sr hydrothermal overprint ages in cratons. Compaction and devolatilization of cover sequence strata during compressive tectonic events along craton margins produce pressurized metasomatic fluids driven towards the craton interior via squeegee-type fluid flow and variations in temperature-pressure gradients. These fluids travel along permeable pathways and crack-seal veins through the cover sequence, migrating into areas of thinner lithosphere within the underlying craton predominantly through critically stressed faults and structural corridors reactivated above the brittle-ductile transition by far-field tectonic stresses (and fluid migration). Pervasive overprint occurs as fluids percolate into reactivated (micro-) fracture networks in granitoid complexes during vertical and horizontal fluid migration along pathways. Structural reactivation does not occur in regions underlain by thick, strong cratonic lithosphere, prohibiting large-scale fluid ingress into these areas and thereby producing the observed spatial distribution of Rb-Sr overprint ages. Further details are provided in the figure annotations and main text.

thicker lithosphere will not because their strength inhibits reactivation. Rather than indicating a lack of structural reactivation, the lack of control by overprint ages by proximal faults (Fig. S9) can be reconciled with the location of samples away from fault damage zones; this suggests that other, smaller structures must be directly responsible for these overprints. While granitoid lithologies are generally regarded as having intrinsically low permeability, residual stresses associated with the crystallization and uplift of a pluton can produce a network of macro- and microfractures, thus providing sufficient bulk permeability to permit fluid flow (Frape et al., 2013; Géraud et al., 2003). As mentioned above, these microfractures manifest in thin sections as transgranular fractures, en-echelon veinlets, and twin-parallel alteration planes in plagioclase and fracture zones. Therefore, these fractures may act as zones of weakness that unseal in response to the same far-field stresses that trigger structural reactivation (e.g., Ramsay, 1980), allowing fluids to travel from reactivated faults into the core of granitoid plutons without the presence of macroscopic veins (cf., Tillberg et al., 2021) (Figs. 4, S10). This fluid flow can also be facilitated by fluid-assisted dissolution of the anorthite component in plagioclase, enabling the formation of micropores/microfractures that pervasively alter plagioclase and contribute to an interconnected fracture network permitting ingress by external fluids (e.g., Yuguchi et al., 2019). Furthermore, the foliation-parallel micro veins in EPT granitoids observed in other studies (e.g., Wiemer et al., 2016) suggest the occurrence of rock cleavage-parallel fracturing of deformed lithologies in response to far-field stresses, providing another pathway for fluid migration.

Regardless of the exact mechanism of transport, crustal fluid-flow events in response to far-field tectonic stress are the most viable explanation for the origin of Rb-Sr overprints observed in Pilbara granitoids. There is no evidence in the geological record of a mantle plume event affecting the Pilbara in the Paleoproterozoic with the capability of heating the crust to thermal overprint. Likewise, delamination of the Pilbara lithosphere during this time is inconsistent with the accepted evolution models for the West Australian Craton (e.g., Cawood and Korsch, 2008). While this is the case for the Pilbara Craton, this does not rule out reset by factors such as plumes, delamination, deformation and basin formation when applying the Rb-Sr system to other cratons.

Our results provide crucial insights into the evolving and ongoing processes that contribute to constructing and assembling cratons and their underlying lithosphere. Critically, these results demonstrate that applying the isotope contour mapping method to Rb-Sr dating of mineral separates can reveal robust spatial and temporal patterns that would otherwise be obscured if using whole-rock Rb-Sr (due to the difference in closure temperatures). Without the large-scale spatial context, isolated ages would yield little information (cf., Fig. 2a). This method shows promise in numerous applications, ranging from diamond exploration to investigations into the post-stabilization histories of Archean cratons. Concerning cratonic stabilization, exemplified by the Pilbara Craton, the production of thick, rigid lithospheric keels does not necessitate a unique and uniform tectonomagmatic setting; their distribution in both Paleo- and Mesoarchean lithotectonic blocks likely indicates diachronous timescales of lithosphere construction even on the scale of tens of kilometres (Figs. 3, 4). The first step in producing thick keels (large-scale mantle depletion) can be protracted upwelling-associated decompression magmatism over a >300 Myr timespan (northeastern EPT) or shorter-lived transtension-driven melting (easternmost Sholl Terrane) (e.g., Vandenburg et al., 2023). These mechanisms produced the necessary degrees of depletion required to impart a high degree of chemical buoyancy upon the underlying lithosphere, which increased viscosity as it cooled. The only step these blocks have in common, amalgamation and lateral compression (e.g., Pearson et al., 2021; Wang et al., 2018), occurred during the 3.06 Ga Prinsep and 2.96–2.92 Ga North Pilbara orogenies (Hickman, 2023) and resulted in the final construction of the lithospheric keel, with cooling inducing gravitational thickening.

5. Conclusions

While it is common for craton margins to experience metamorphism during amalgamation with younger mobile belts (e.g., Superior Craton – Grenville Orogeny, Rae and Hearne Cratons – Trans-Hudson Orogeny (Weller et al., 2021); Yilgarn and Pilbara Cratons – Capricorn Orogen sequence, Yilgarn Craton – Albany-Fraser Orogen (Cawood and Korsch, 2008)), widespread protracted, largely deformation-absent post-cratonization metamorphism in stable

craton interiors has not been previously reported. We demonstrate that lithospheric architecture profoundly impacts fluid-borne metamorphism in cratons long after tectonic stabilization. Whereas a craton can still be considered stable and, therefore, able to withstand the forces of destruction, the resetting of ages linked to variations in craton-scale lithospheric thickness can only be achieved through large-scale fluid flow, which in itself is a reflection of lithospheric resistance to far-field tectonic stresses. Fluid flow is widely associated with elemental redistribution within the crust and need not be triggered by proximal tectonomagmatic events; distal tectonic compression can also drive fluids deep into a craton (e.g., Tillberg et al., 2021; Rasmussen et al., 2023). Contrary to popular belief, our results demonstrate that cratons (especially granitoid complexes) can be quite permeable and behave as crustal "sponges" in response to orogenic fluid flow events. Thus, in addition to providing a viable upgrading mechanism for iron formations (e.g., White et al., 2014) and source fluids for unconformity-hosted uranium deposits and sediment-hosted massive sulfide deposits (e.g., Pirajno, 2009) in cratonic cover sequences, the unexpectedly large footprints of these fluid flow events also provide conditions favourable to the formation of hydrothermal ore deposits in the underlying granite-greenstone basement (Huston et al., 2002) for billions of years after stabilization. Although the widespread application of the Rb-Sr system to Archean igneous rocks has previously fallen out of favour, its use as a "geochemical x-ray" provides important snapshots of some of Earth's oldest lithosphere, thereby bolstering its renaissance.

CRediT authorship contribution statement

Eric D. Vandenburg: Writing – review & editing, Writing – original draft, Visualization, Validation, Methodology, Investigation, Formal analysis, Data curation, Conceptualization. **Oliver Nebel:** Writing – review & editing, Supervision, Resources, Methodology, Investigation, Funding acquisition, Conceptualization. **Peter A. Cawood:** Writing – review & editing, Supervision, Resources, Investigation, Funding acquisition. **R. Hugh Smithies:** Writing – review & editing, Supervision, Resources, Investigation. **Fabio A. Capitanio:** Writing – review & editing, Investigation. **Laura A. Miller:** Writing – review & editing, Investigation. **Marc-Alban Millet:** Writing – review & editing, Investigation. **Emilie Bruand:** Writing – review & editing, Investigation. **Jean-François Moyen:** Writing – review & editing, Investigation. **Xueying Wang:** Writing – review & editing, Validation, Resources, Methodology, Investigation. **Massimo Raveggi:** Writing – review & editing, Validation, Resources, Methodology, Investigation. **Yona Jacobsen:** Writing – review & editing, Supervision, Resources, Methodology, Conceptualization.

Declaration of competing interest

The authors declare that they have no known competing financial interests or personal relationships that could have appeared to influence the work reported in this paper.

Data availability

All data needed to evaluate the conclusions in the paper are present in the paper and/or the Supplementary Materials.

Acknowledgements

First and foremost, we are grateful to Frederic Moynier for editorial handling and Graham Pearson and Tim Johnson for their constructive and insightful reviews of this manuscript. We thank Chris Voisey for conversations about structural permeability, Bruno Ribeiro for assistance with analyses, Junnel Alegado for assistance with sample preparation, and David Champion for providing contextual information on GA repository samples. RHS publishes with the permission of the Executive Director of the Geological Survey of Western Australia.

Funding: ON and PAC acknowledge funding from the Australian Government through Australian Research Council Discovery (DP180100580) and Laureate Fellowship (FL160100168) projects, respectively. MAM acknowledges support from NERC standard grant NE/R001332/1.

Appendix A. Supplementary material

Supplementary material related to this article can be found online at https://doi.org/10.1016/j.epsl.2023.118401.

References

Attendorn, H.-G., Bowen, R.N.C., 1997. Rubidium-strontium dating. In: Radioactive and Stable Isotope Geology. Springer, Netherlands, pp. 159–191.
Bedle, H., Cooper, C.M., Frost, C.D., 2021. Nature versus nurture: preservation and destruction of Archean Cratons. Tectonics 40, 1–38.
Bekker, A., Krapež, B., Karhu, J.A., 2020. Correlation of the stratigraphic cover of the Pilbara and Kaapvaal cratons recording the lead up to Paleoproterozoic Icehouse and the GOE. Earth-Sci. Rev. 211, 103389.
Bhaskar Rao, Y.J., Sivaraman, T.V., Pantulu, G.V.C., Gopalan, K., Naqvi, S.M., 1992. Rb-Sr ages of late Archean metavolcanics and granites, Dharwar craton, South India and evidence for Early Proterozoic thermotectonic event (s). Precambrian Res. 59, 145–170.
Braun, J., Shaw, R., 2001. A thin-plate model of Palaeozoic deformation of the Australian lithosphere: implications for understanding the dynamics of intracratonic deformation. Geol. Soc. Spec. Publ. 184, 165–193.
Brown, M.C., Oliver, N.H.S., Dickens, G.R., 2004. Veins and hydrothermal fluid flow in the Mt. Whaleback Iron Ore District, eastern Hamersley Province, Western Australia. Precambrian Res. 128, 441–474.
Capitanio, F.A., Nebel, O., Cawood, P.A., 2020. Thermochemical lithosphere differentiation and the origin of cratonic mantle. Nature 588, 89–94.
Carlson, R.W., 2011. Absolute age determinations: radiometric. In: Gupta, H.K. (Ed.), Encyclopedia of Solid Earth Geophysics. Springer Nature, Switzerland, pp. 1–8.
Cawood, P.A., Korsch, R.J., 2008. Assembling Australia: proterozoic building of a continent. Precambrian Res. 166, 1–35.
Cawood, P.A., et al., 2022. Secular evolution of continents and the Earth system. Rev. Geophys. 60.
Cooper, C.M., Lenardic, A., Levander, A., Moresi, L., 2006. Creation and preservation of cratonic lithosphere: seismic constraints and geodynamic models. In: Archean Geodynamics and Environments. American Geophysical, Union (AGU), pp. 75–88.
Cox, S.F., 2005. Coupling between deformation, fluid pressures, and fluid flow in ore-producing hydrothermal systems at depth in the crust. In: One Hundredth Anniversary Volume. Society of Economic Geologists, pp. 39–75.
Czarnota, K., Roberts, G.G., White, N.J., Fishwick, S., 2014. Spatial and temporal patterns of Australian dynamic topography from river profile modeling. J. Geophys. Res., Solid Earth 119, 1384–1424.
Dhuime, B., Hawkesworth, C.J., Cawood, P.A., Storey, C.D., 2012. A change in the geodynamics of continental growth 3 billion years ago. Science 335, 1334–1336.
Dodson, M.H., 1973. Closure temperature in cooling geochronological and petrological systems. Contrib. Mineral. Petrol. 40, 259–274.
Fielding, I.O.H., et al., 2017. Using in situ SHRIMP U-Pb monazite and xenotime geochronology to determine the age of orogenic gold mineralization: an example from the Paulsens Mine, Southern Pilbara Craton. Econ. Geol. 112, 1205–1230.
Fishwick, S., Rawlinson, N., 2012. 3-D structure of the Australian lithosphere from evolving seismic datasets. Aust. J. Earth Sci. 59, 809–826.
Fitz Gerald, J.D., Stünitz, H., 1993. Deformation of granitoids at low metamorphic grade. I: reactions and grain size reduction. Tectonophysics 221, 299–324.
Flowers, R.M., Bowring, S.A., Mahan, K.H., Williams, M.L., Williams, I.S., 2008. Stabilization and reactivation of cratonic lithosphere from the lower crustal record in the western Canadian shield. Contrib. Mineral. Petrol. 156, 529–549.
Frape, K., et al., 2013. Deep Fluids in the Continents, 2nd ed. Elsevier Ltd.
Géraud, Y., Surma, F., Mazerolle, F., 2003. Porosity and fluid flow characterization of granite by capillary wetting using X-ray computed tomography. Geol. Soc. (Lond.) Spec. Publ. 215, 95–105.
Groshong, R.H., 1990. Low-temperature deformation mechanisms and their interpretation. Spec. Pap., Geol. Soc. Am. 253, 337–368. https://doi.org/10.1130/SPE253-p337.
Harrison, T.M., Armstrong, R.L., Naeser, C.W., Harakal, J.E., 1979. Geochronology and thermal history of the Coast Plutonic Complex, near Prince Rupert, British Columbia. Can. J. Earth Sci. 16, 400–410.

Herzberg, C., Rudnick, R., 2012. Formation of cratonic lithosphere: an integrated thermal and petrological model. Lithos 149, 4–15.
Hickman, A.H., 2023. Archean Evolution of the Pilbara Craton and Fortescue Basin. Springer International Publishing.
Hoggard, M.J., et al., 2020. Global distribution of sediment-hosted metals controlled by craton edge stability. Nat. Geosci. 13, 504–510.
Hogmalm, K.J., Zack, T., Karlsson, A.K.-O., Sjöqvist, A.S.L., Garbe-Schönberg, D., 2017. In situ Rb–Sr and K–Ca dating by LA-ICP-MS/MS: an evaluation of N_2O and SF_6 as reaction gases. J. Anal. At. Spectrom. 32, 305–313.
Huston, D.L., et al., 2002. The timing of mineralization in the Archean North Pilbara terrain, Western Australia. Econ. Geol. 97, 733–755.
Jordan, T.H., 1988. Structure and formation of the continental tectosphere. J. Petrol. Special Volume, 11–37.
Lee, C.T.A., Luffi, P., Chin, E.J., 2011. Building and destroying continental mantle. Annu. Rev. Earth Planet. Sci. 39, 59–90.
Lenardic, A., Moresi, L.-N., 1999. Some thoughts on the stability of cratonic lithosphere: effects of buoyancy and viscosity. J. Geophys. Res., Solid Earth 104, 12747–12758.
Liebmann, J., Kirkland, C.L., Kelsey, D.E., Korhonen, F.J., Rankenburg, K., 2022. Lithological fabric as a proxy for Rb–Sr isotopic complexity. Chem. Geol. 608, 1–15.
Liu, J., Cai, R., Pearson, D.G., Scott, J.M., 2019. Thinning and destruction of the lithospheric mantle root beneath the North China Craton: a review. Earth-Sci. Rev. 196, 102873.
Lyubetskaya, T., Ague, J.J., 2009. Modeling the magnitudes and directions of regional metamorphic fluid flow in collisional orogens. J. Petrol. 50, 1505–1531.
Martin, D.M.B., Hocking, R.M., Riganti, A., Tyler, I.M., 2015. Geological Map of Western Australia 1:2 500 000. Geological Survey of Western Australia, 000.
Mole, D.R., et al., 2018. The Archean Fortescue large igneous province: a result of komatiite contamination by a distinct Eo-Paleoarchean crust. Precambrian Res. 310, 365–390.
Oliver, J., 1992. The spots and stains of plate tectonics. Earth-Sci. Rev. 32, 77–106.
Oversby, V.M., 1976. Isotopic ages and geochemistry of Archaean acid igneous rocks from the Pilbara, Western Australia. Geochim. Cosmochim. Acta 40, 817–829.
Pearson, D.G., et al., 2021. Deep continental roots and cratons. Nature 596, 199–210.
Perchuk, A.L., Gerya, T.V., Zakharov, V.S., Griffin, W.L., 2020. Building cratonic keels in Precambrian plate tectonics. Nature 586, 395–401.
Pirajno, F., 2009. Hydrothermal Processes and Mineral Systems. Springer, Netherlands.
Poudjom Djomani, Y.H., Derek Fairhead, J., Griffin, W.L., 1999. The flexural rigidity of Fennoscandia: reflection of the tectonothermal age of the lithospheric mantle. Earth Planet. Sci. Lett. 174, 139–154.
Raimondo, T., Hand, M., Collins, W.J., 2014. Compressional intracontinental orogens: ancient and modern perspectives. Earth-Sci. Rev. 130, 128–153. https://doi.org/10.1016/j.earscirev.2013.11.009.
Ramsay, J.G., 1980. The crack–seal mechanism of rock deformation. Nature 284, 135–139.
Rasmussen, B., Fletcher, I.R., Sheppard, S., 2005. Isotopic dating of the migration of a low-grade metamorphic front during orogenesis. Geology 33, 773.
Rasmussen, B., Fletcher, I.R., Muhling, J.R., 2007. In situ U–Pb dating and element mapping of three generations of monazite: unravelling cryptic tectonothermal events in low-grade terranes. Geochim. Cosmochim. Acta 71, 670–690.
Rasmussen, B., Zi, J., Muhling, J., 2022. U-Pb dating reveals multiple Paleoproterozoic orogenic events (Hamersley orogenic cycle) along the southern Pilbara margin (Australia) spanning the onset of atmospheric oxygenation. Geology 50, 959–963.
Rasmussen, B., Zi, J., Muhling, J.R., 2023. Tectonic fluid expulsion: U-Pb evidence for punctuated hydrothermal fluid flow and hydraulic fracturing during orogenesis. Earth Planet. Sci. Lett. 604, 117997.
Sheppard, S., Occhipinti, S.A., Nelson, D.R., 2005. Intracontinental reworking in the Capricorn Orogen, Western Australia: the 1680–1620 Ma Mangaroon Orogeny*. Aust. J. Earth Sci. 52, 443–460.
Sheppard, S., Krapež, B., Zi, J.W., Rasmussen, B., Fletcher, I.R., 2017. Young ores in old rocks: Proterozoic iron mineralisation in Mesoarchean banded iron formation, northern Pilbara Craton, Australia. Ore Geol. Rev. 89, 40–69.
Siler, D.L., Kennedy, B.M., 2016. Regional crustal-scale structures as conduits for deep geothermal upflow. Geothermics 59, 27–37.
Sleep, N.H., 2003. Survival of Archean cratonal lithosphere. J. Geophys. Res., Solid Earth 108, 1–29.
Smithies, H.R., Champion, D.C., Sun, S.S., 2004. The case for Archaean boninites. Contrib. Mineral. Petrol. 147, 705–721.
Steinberger, B., Becker, T.W., 2018. A comparison of lithospheric thickness models. Tectonophysics 746, 325–338.
Tesauro, M., Kaban, M.K., Cloetingh, S.A.P.L., 2012. Global strength and elastic thickness of the lithosphere. Glob. Planet. Change 90–91, 51–57.
Thorne, A.M., Trendall, A.F., 2001. Geology of the Fortescue Group.
Tillberg, M., et al., 2021. Reconstructing craton-scale tectonic events via in situ Rb-Sr geochronology of poly-phased vein mineralization. Terra Nova 33, 502–510.
Townend, J., Zoback, M.D., 2000. How faulting keeps the crust strong. Geology 28, 399–402.
Vandenburg, E.D., et al., 2023. Spatial and temporal control of Archean tectonomagmatic regimes. Earth-Sci. Rev. 241, 104417.
Wang, C., et al., 2022. Advances in in-situ Rb-Sr dating using LA-ICP-MS/MS: applications to igneous rocks of all ages and to the identification of unrecognized metamorphic events. Chem. Geol. 610, 121073.
Wang, H., van Hunen, J., Pearson, D.G., 2018. Making Archean cratonic roots by lateral compression: a two-stage thickening and stabilization model. Tectonophysics 746, 562–571.
Weller, O.M., et al., 2021. The metamorphic and magmatic record of collisional orogens. Nat. Rev. Earth Environ. 2, 781–799.
White, A.J.R., Smith, R.E., Nadoll, P., Legras, M., 2014. Regional-scale metasomatism in the Fortescue Group Volcanics, Hamersley Basin, Western Australia: implications for hydrothermal ore systems. J. Petrol. 55, 977–1009.
Wiemer, D., Schrank, C.E., Murphy, D.T., Hickman, A.H., 2016. Lithostratigraphy and structure of the early Archaean Doolena Gap greenstone belt, East Pilbara Terrane, Western Australia. Precambrian Res. 282, 121–138.
Willigers, B.J.A., Mezger, K., Baker, J.A., 2004. Development of high precision Rb–Sr phlogopite and biotite geochronology; an alternative to $^{40}Ar/^{39}Ar$ tri-octahedral mica dating. Chem. Geol. 213, 339–358.
Yuguchi, T., Shoubuzawa, K., Ogita, Y., Yagi, K., Ishibashi, M., Sasao, E., Nishiyama, T., 2019. Role of micropores, mass transfer, and reaction rate in the hydrothermal alteration process of plagioclase in a granitic pluton. Am. Mineral. 104, 536–556.
Zack, T., Hogmalm, K.J., 2016. Laser ablation Rb/Sr dating by online chemical separation of Rb and Sr in an oxygen-filled reaction cell. Chem. Geol. 437, 120–133.